Sliding Mode-based Model Predictive Control of Grid-Forming Power Converters

Oshnoei, Arman; Blaabjerg, Frede

Published in:
Proceedings of the 2023 European Control Conference (ECC)

DOI (link to publication from Publisher):
10.23919/ECC57647.2023.10178243

Publication date:
2023

Document Version
Accepted author manuscript, peer reviewed version

Sliding Mode-based Model Predictive Control of Grid-Forming Power Converters

Arman Oshnoei[1] and Frede Blaabjerg[1]

Abstract— **Grid-forming (GFM) converters are becoming an inevitable component of AC power systems due to the growing demand for distributed energy resources. However, enhancing their performance is still a critical challenge. Conventional dual-loop proportional-integral (PI) control structures are usually used to control a GFM inverter in a *dq* reference frame. However, they experience unbalancing in transient and steady-state performance. This paper proposes a sliding-mode control (SMC) based finite control set model predictive control (FCS-MPC) for voltage control of a GFM inverter in a grid-connected mode. The SMC is presented for the adaptive and optimal determination of the weighting factors in FCS-MPC. The proposed strategy's key benefit is the SMC's real-time execution. By doing this, the weighting factors are constantly updated in real-time, which avoids the dependence of the response of the inverter control system under uncertainties and external disturbances. Furthermore, to accurately track power references and deliver the required virtual inertia, a virtual synchronous generator controller is utilized to implement the active power loop. The suggested approach has been shown to be effective based on the simulation results when compared to a dual-loop PI control method.**

I. INTRODUCTION

Grid-forming (GFM) inverters can regulate the grid voltage and frequency more effectively than synchronous machines when operating as voltage-controlled sources due to their fast response and enhanced controllability [1]-[3]. Many advanced control techniques and topologies for GFM inverters have been suggested in recent years. The voltage regulation of a GFM inverter is typically executed using a dual-loop structure formed of linear controllers [4]-[6]. Even though they are simple to understand and simple to use, they operate poorly when the output frequency varies and exhibit unbalancing in transient and steady-state performance. In applications such as hierarchically organized microgrids, a dual-loop structure requires the outer voltage loop to have a significantly lower bandwidth than the inner current loops. As a result, there is a natural limitation on bandwidth that can negatively impact the efficiency of higher regulation layers [7], [8].

To cover the cited drawbacks, recent research has indicated that Finite Control Set Model Predictive Control (FCS-MPC) could be a viable substitute for traditional methods in regulating the voltage of GFM inverters due to its capability to handle multiple objectives and constraints [5], [9], [10]. The FCS-MPC utilizes a limited number of voltage source inverter (VSI) switching combinations to enable the prediction model to estimate the output generated by each switch combination. An objective function (OF) is then employed to obtain the optimal switching states of the VSI. Recent investigations have revealed that FCS-MPC is an efficient alternative to traditional controllers in inverter voltage regulation [2], [6], [11], [12]. Nevertheless, these studies addressed this problem once the GFM inverter operates only in a standalone mode.

The performance of the FCS-MPC is heavily influenced by the weighting factors (WFs) incorporated in the objective function (OF), which can be difficult to tune. Numerous efforts have been made to tackle this problem. Some offered to withdraw the WF. The OFs without WF can be attained by combining the control purposes' dimensions [13], or dividing the problem into two OFs [14]-[16]. Including WFs, however, cannot always be bypassed, as the number of objectives is so much which is difficult to be unified. To calculate the WFs, techniques that employ artificial intelligence [17]-[20], genetic algorithms [21], and fuzzy control [22] were proposed. On the other hand, the approach presented in [17] employs an offline computation process of the WF and the flux reference, achieving a quick drive start and satisfactory response under various loading scenarios. The design procedure is simple and practical for different OFs [23]. However, the extra memory requirement to save the estimated WFs is the cost of the offline calculations. Furthermore, those studies' analyses used to determine the optimal values of WFs depend on the operating conditions, which could result in an unsatisfactory performance.

Accordingly, this paper employs the FCS-MPC for voltage control of a GFM inverter in a grid-connected mode. To avoid relying on the inverter control system's response to the operating scenarios, the WFs emerging in the FCS-MPC's OF are obtained online via a sliding mode (SMC) approach. The major feature of the proposed control scheme is the capability to generate dynamic outputs for control objectives. Also, to maintain damping, inertia, and droop characteristics while following power references, a virtual synchronous generator (VSG) controller is executed in the active power loop (APC), and the parameters of the VSG system are obtained through small signal analysis. Simulation validations are offered to verify the suggested control method's effectiveness.

The rest of this paper is categorized as follows. First, Section II covers the system description, including the VSG

*This work was supported by the Reliable Power Electronic-Based Power Systems (REPEPS) project at the AAU Energy Department, Aalborg University, as a part of the Villum Investigator Program funded by the Villum Foundation.

[1]Arman Oshnoei and Frede Blaabjerg are with the Department of Energy, Aalborg University, 9220 Aalborg, Denmark aros@energy.aau.dk, fbl@energy.aau.dk

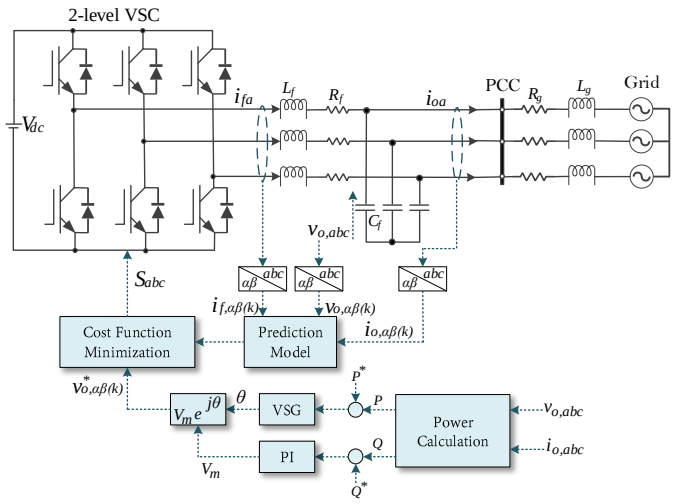

Fig. 1. Schematic of the presented system

Controller and test system. In section III, the principle of the FCS-MPC for GFM inverter control is introduced. Then, section IV deals with the design process of the SMC to tune the WFs in the FCS-MPC. The simulation results under two operational cases are ¨presented in section V. Section VI provides a summary that concludes the paper.

II. SYSTEM DESCRIPTION

A. Test System

The system layout used to assess the suggested control strategy is illustrated in Fig. 1. It comprises a GFM inverter linked to the grid at the point of common coupling (PCC) via a three-phase LC filter, which is utilized to remove the harmonics of the output voltage and current. C_f and L_f are capacitance and inductance of the LC filter. An RL branch ($Z_g = R_g + j\omega L_g$) emulates the grid impedance. The system execution includes a voltage source inverter with the inner current and voltage regulation using PI controllers in *dq* frame. To regulate the voltage of the GFM inverter, in the control system, the reactive power control loop incorporates a PI controller [24], whereas the active power control loop employs the VSG strategy to furnish virtual inertia and damping. The VSG control strategy mimics the synchronous generator behavior via a swing equation [25].

B. VSG Controller

The control diagram of the VSG system is illustrated in Fig. 2. According to Fig. 2, the closed-loop transfer function ($G_{cl}(s)$) is derived as

$$G_{cl}(s) = \frac{\frac{v_o v_g}{J\omega_o X_g}}{s^2 + (\frac{D}{J\omega_o})s + \frac{v_o v_g}{J\omega_o X_g}} \tag{1}$$

where v_g and v_o are the RMS values of the grid and capacitance voltages, respectively; $X_g = \omega L_g$ is the grid reactance; J, D, and ω_o are rotational inertia, damping factor, and nominal frequency, respectively. Eq. (1) can be expressed

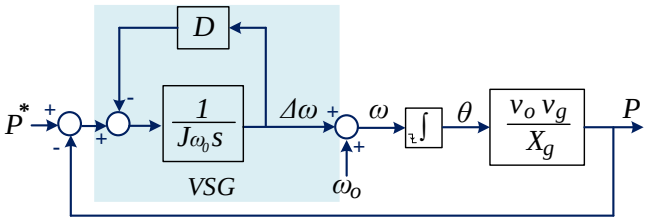

Fig. 2. Structure of the VSG controller

as a generalized second-order equation as below

$$G_{cl}(s) = \frac{\omega_n^2}{s^2 + 2\xi\omega_n s + \omega_n^2} \tag{2}$$

where $\omega_n = \sqrt{\frac{v_o v_g}{J\omega_o X_g}}$ and $\xi = \frac{D}{2\sqrt{\frac{v_o v_g J\omega_o}{X_g}}}$. ω_n and ξ referred to as the closed-loop system's natural frequency and damping ratio, respectively. The closed-loop system's damping and bandwidth are impacted by ξ and ω_n, respectively. Therefore, D and J influence the overshoot and rise-time of the system's step response in the grid-connected mode directly. Besides, the frequency dynamics to a change in load value in the standalone mode can be written as follows:

$$\Delta\omega = \frac{-D}{(J\omega_o D s + 1)}.\Delta P_l \tag{3}$$

where ΔP_l is the variation in load value. The inertia constant H is frequently used to denote the inertia properties instead of inertial moment J, which is defined by:

$$H = \frac{J{\omega_0}^2}{2S_r}. \tag{4}$$

where S_r is the inverter rating. Table I contains the system parameters. The step response of (2) in the grid-connected mode and (3) in the standalone mode are shown in Fig. 3. As seen, an increased H will result in more inertia support. Thus, a larger H is anticipated from inertia's viewpoint. Nevertheless, an increased H implies additional energy is drawn from the energy source to support inertia, as plotted in Fig. 3. Thus, adjusting the parameters of the VSG controller to reach control purposes in both grid-connected and stand-alone modes is a challenging task. Here, H is chosen according to the SG's inertia constant with the same power level [26]. ζ is chosen as 0.707, which can ensure the settling time and overshoot are in the desired range.

III. FINITE CONTROL SET-MODEL PREDICTIVE CONTROL

Inverters' conventional PI-based inner controller has three cascaded control parts to guarantee frequency and voltage frequency stability, the current and voltage control loops, and PWM. To enhance the VSI's dynamic performance, the FCS-MPC is presented as the voltage regulator. The impact of low bandwidth in current and voltage loops can be withdrawn using the FCS-MPC controller [5]. Thus, more bandwidth flexibility and rapid dynamic reaction can be reached by substituting the FCS-MPC with the dual-loop

TABLE I

PARAMETERS OF THE SYSTEM

Parameters	Description	Value
v_g	Grid voltage (RMS)	70 V
ω_0	Nominal frequency	100π rad/s
L_g and R_g	Line impedance	3.6 mH and 0.2 Ω
L_f and C_f	LC-filter	2.4 mH and 15 μF
r_v and x_v	Virtual impedance	-0.2 Ω and 0.8 Ω
S_r	Inverter rating	1 kW
SCR	Short circuit ratio	4.3
V_{dc}	DC-side voltage	200 V
T_s	Sampling time	20 μs

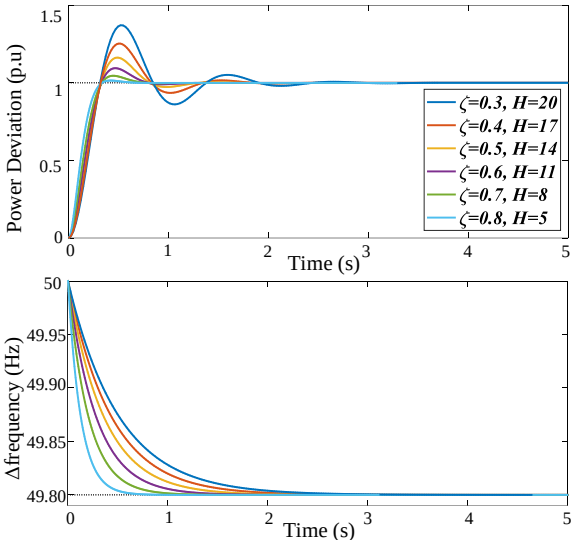

Fig. 3. Step response of: (a) (2) in the grid-connected mode and (b) (3) in the standalone mode.

PI-based structure. To operate, the FCS-MPC calculates an OF for all possible switching modes of the VSI and then selects the optimal v_i that minimizes the OF while taking constraints into account. Fig. 4 shows voltage vectors and eight possible switching states where each vector yields a distinct OF. Although OF_0 and OF_7 have the same value, their impacts on the switching orders (number of on/off switches used throughout each cycle) and switching losses' value are different.

The schematic of the FCS-MPC is shown in Fig. 1. The output current, output voltage, and filter current (i_o, v_o, i_f) are given in vectors as below:

$$i_o=[i_{ou}, i_{ov}, i_{ow}]^T,\ i_f=[i_{fu}, i_{fv}, i_{fw}]^T,\ v_o=[v_{cu}, v_{cv}, v_{cw}]^T \tag{5}$$

By employing the Clarke transformation, three-phase state variables are converted to a two-dimensional vector.

Finally, the converter's output current and voltage are illustrated by the differential equation shown below.

$$\frac{d}{dt}\begin{bmatrix} i_f \\ v_o \end{bmatrix} = \begin{bmatrix} -\frac{R_f}{L_f} & -\frac{1}{L_f} \\ \frac{1}{C_f} & 0 \end{bmatrix}\begin{bmatrix} i_f \\ v_o \end{bmatrix} + \begin{bmatrix} \frac{1}{L_f} & 0 \\ 0 & -\frac{1}{C_f} \end{bmatrix}\begin{bmatrix} v_i \\ i_o \end{bmatrix} \tag{6}$$

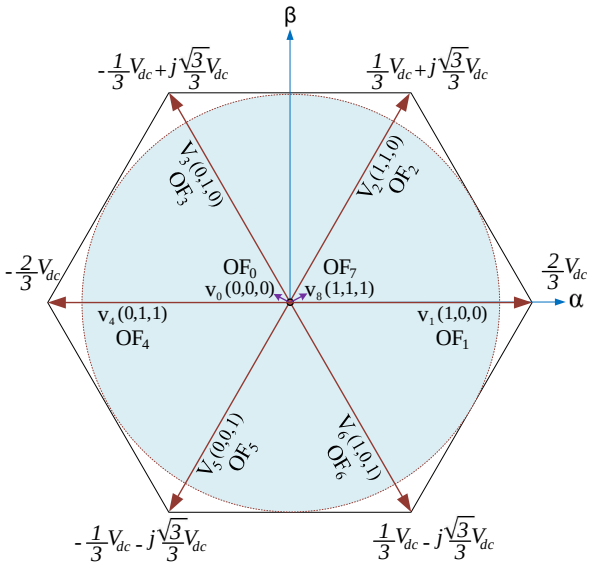

Fig. 4. Voltage vectors and switching states.

If i_o is regarded as a measured disturbance and v_i as the control input, the discrete-time state-space representation at time step k can be expressed as:

$$x(k+1) = Ax(k) + Bv_i(k) + Fi_o(k) \tag{7}$$

in which

$$\mathbf{A} = \begin{bmatrix} -\frac{R_f}{L_f} & -\frac{1}{L_f} \\ \frac{1}{C_f} & 0 \end{bmatrix},\ \mathbf{B} = \begin{bmatrix} \frac{1}{L_f} \\ 0 \end{bmatrix},\ \mathbf{F} = \begin{bmatrix} 0 \\ -\frac{1}{C_f} \end{bmatrix} \tag{8}$$

The FCS-MPC aims to achieve precise regulation of v_i to enable the output voltage $v_o = v_{o,\alpha} + jv_{o,\beta}$ to accurately track the reference voltage $v_o^* = v_{o,\alpha}^* + jv_{o,\beta}^*$. The OF is expressed as [12]:

$$OF = (v_{o,\alpha}^* - v_{o,\alpha})^2 + (v_{o,\beta}^* - v_{o,\beta})^2 + \delta_w SW^2 \tag{9}$$

The converter's switching effort is limited by a weighting factor (δ_w) in which $SW = ||v_i(k) - v_i(k-1)||$. However, in order to improve the voltage regulation performance of the VSC, the OF in (11) can be modified to incorporate the error related to the output voltage derivative. This error can be computed as shown below [12]:

$$G_{der} = (C_f\omega^* v_{o,\alpha}^* - i_{f,\alpha} + i_{o,\alpha})^2 + (C_f\omega^* v_{o,\beta}^* + i_{f,\beta} - i_{o,\beta})^2 \tag{10}$$

where $\omega^* = 2\pi f_r$ is the angular frequency of the reference voltage.

Adding the term in (11), multiplied by the factor δ_{der}, results in a modified OF

$$OF = (v_{o,\alpha}^* - v_{o,\alpha})^2 + (v_{o,\beta}^* - v_{o,\beta})^2 + \delta_w SW^2 + \delta_{der} G_{der} \tag{11}$$

It is clear that the WF (δ_w and δ_{der}) have a substantial influence on the system's performance. In this paper, the SMC method is employed to adjust WF quickly and online, enhancing the converter control system's performance. The next section discusses the SMC-based regulation scheme's design process.

IV. SLIDING MODE CONTROL APPROACH

There are two phases in the SMC design; the design surface in the state space is the initial phase, known as a sliding surface. The second phase is the control rule design that relates the slip surface to the state variables [1], [27].

A. Sliding surface (SS)

The SS is an area of the state space where it is ensured that the system will behave in a predefined and stable manner. Therefore, the sliding surface's stability demands the choice of a generalized Lyapunov function (positive definite), where the time derivative in the surface attraction area is negative. In this study, a non-linear surface is chosen to assure the system functions as expected and is resistant to disturbances. According to [28], the SS is given as below:

$$\sigma(x,t) = (\frac{d}{dt} + \eta_b)e(x,t) \tag{12}$$

where $e(x,t)$ is the difference between the variable state and reference; and η_b is a positive surface constant. The proposed SS used for the FCS-MPC's coefficients design can be described from (12) as follows

$$\sigma = [\alpha \;\; \beta] \begin{bmatrix} x_1 \\ x_2 \end{bmatrix} = \alpha x_1 + \beta x_2 \tag{13}$$

where σ denotes the sliding surface; α and β are the real and positive constants. The Lyapunov stability criteria inflict the state $\dot{V} = \sigma\dot{\sigma} \leq 0$, which results in

$$\dot{\sigma} = \alpha\dot{x_1} + \beta\dot{x_2} \leq 0 \tag{14}$$

From the (8), x_1 and x_2 can be expressed as:

$$\begin{aligned} x_1 &= i_f^* - i_f \\ x_2 &= v_o^* - v_o \end{aligned} \tag{15}$$

where $i_f^* = C_f\omega^* v_o^* + i_o$.

B. Control law

It is essential for the control rule to meet the requirements for both reachability and existence in the sliding mode. The control rule must fulfill the reachability and existence requirements in the sliding mode. Since the FCS-MPC contains two weighting factors (δ_{der} and δ_w), hence two SMC controllers are developed.

The proposed control input to meet (14) is expressed as

$$C_{s1} = -ax_1 - LPF(\gamma_1 sgn(\sigma)) \tag{16}$$

where $\gamma_1 = \delta_{der} + \delta_{der,0}$, in which $\delta_{der,0}$ is the initial value of WF corresponding to (11), $LPF(\cdot)$ is a first-order low-pass filter employed to alleviate the SMC chattering, and $sgn(\cdot)$ is a signum function which is represented by

$$sgn(\sigma) = \begin{cases} -1 & if \quad \sigma < 0 \\ 0 & if \quad \sigma = 0 \\ 1 & if \quad \sigma > 0 \end{cases} \tag{17}$$

Similarly, for the second SMC controller, control input is written as follow:

$$C_{s2} = -bx_2 - LPF(\gamma_2 sgn(\sigma)) \tag{18}$$

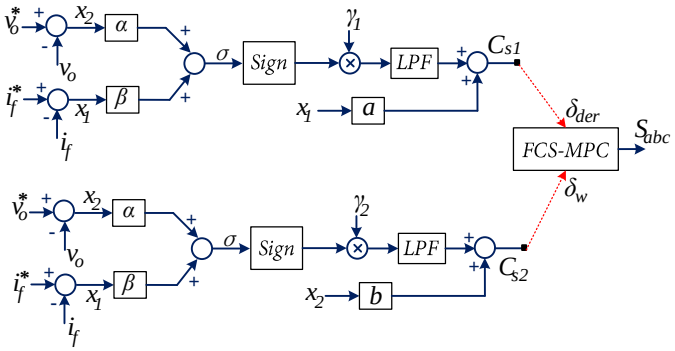

Fig. 5. Structure of the proposed SMC-based regulation scheme for WFs in FCS-MPC.

where a and b are the controller's parameters; $\gamma_2 = \delta_w + \delta_{w,0}$, in which $\delta_{w,0}$ is the initial value of WF corresponding to switching effort. Fig. 5 depicts the schematic of the presented SMC-based regulation strategy for WFs in FCS-MPC.

V. EXPERIMENTAL RESULTS

The proposed method is verified using a GFM inverter laboratory setup carried out based on the schematic depicted in Fig. 1. Further details about the experimental setup can be found in [1]. The parameters utilized in the model are listed in Table I.

A. Examination of voltage harmonics at the PCC

To analyze the effect of the proposed approach on the total harmonic distortion (THD) of output voltages, an analysis is carried out utilizing the inverter's switching model. In this analysis, an uncertainty is introduced in i_f, which is modeled using a uniform distribution with lower and upper limits of 2% to the absolute value of the actual value. For instance, if the current value is 1 (A), after adding the uniform disturbance, the current changes in the interval of [0.95, 1.05]. The PCC voltage tracking behavior of the proposed controller and the traditional dual-loop PI method is illustrated in Fig. 6. The PI controller is adjusted according to the strategy given in [1]. Based on IEEE Standard 519-2014, in low (middle) voltage applications where the PCC voltage is less than 69 kV, the THD of the output voltages should be less than 8% (5%). It is worth mentioning that the average value of total harmonic distortions (THDs) of three-phase output voltage is reported on the output voltage plots (Vo, abc). The THD analysis shows that the proposed method yields a THD value of 3.5%, which is lower than the THD value of 6.3% obtained using the classical dual-loop PI method. The generated WFs by SMC are exhibited in Fig. 7. Figure 8 illustrates the frequency spectrum characteristics of the a-phase output voltage (Vo, a) obtained using the conventional PI method and the proposed method.

B. Verification for active power control loop

This test assesses the VSG system's performance in grid-connected mode by accurately following the specified power reference actions. Initially, the GFM inverter and grid are

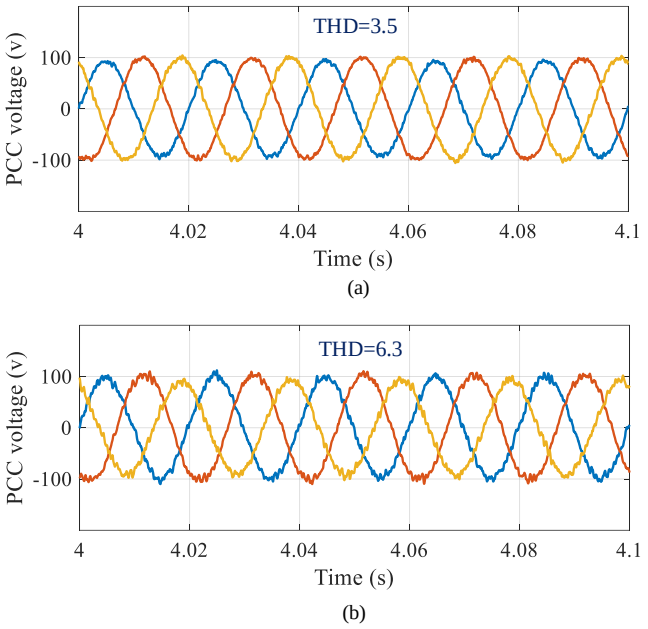

Fig. 6. The PCC voltage waveforms: (a) proposed control scheme; (b) conventional PI method.

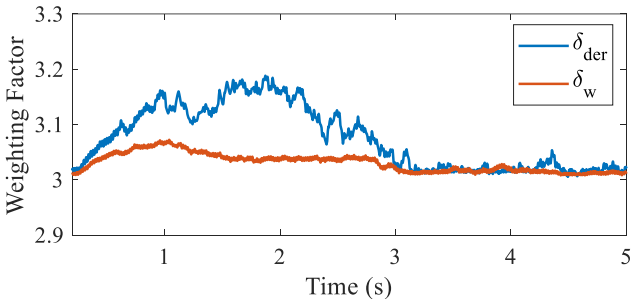

Fig. 7. The generated WFs by the proposed SMC strategy.

synchronized by setting reference powers to $P^{=}100$ and $Q^{=}100$, respectively. Fig. 9 (a) shows the active power and frequency changes when the reference active power steps from 100 W to 600 W at $t \approx 29.3s$, then to 400 W at $t \approx 69.3s$, and eventually to 800 W at $t \approx 89.3s$. Fig. 9 (b) presents the active power and frequency changes when the reference voltage decreases from 1 p.u. to 0.9 p.u. As demonstrated in both figures, the presented APC loop is capable of accurately tracking the specified references during transient operations. Additionally, the figures indicate that the overshoot and settling time of the active power and frequency deviations are within acceptable ranges. In the context of step responses, overshoot refers to the highest value achieved, and settling time is the duration over which the response remains within 2% of the steady-state value.

VI. CONCLUSIONS

This paper proposed an approach based on FCS-MPC for voltage control of a GFM inverter. An SMC-based approach was proposed to provide real-time and adaptive adjustment of the WF of the FCS-MPC. The main advantage

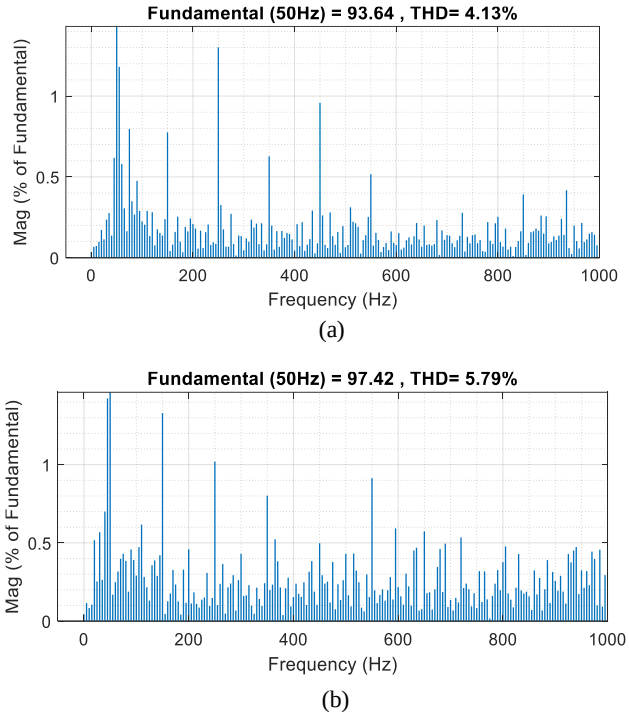

Fig. 8. Frequency spectrum features of a-phase output voltage: (a) proposed control scheme; (b) conventional PI method.

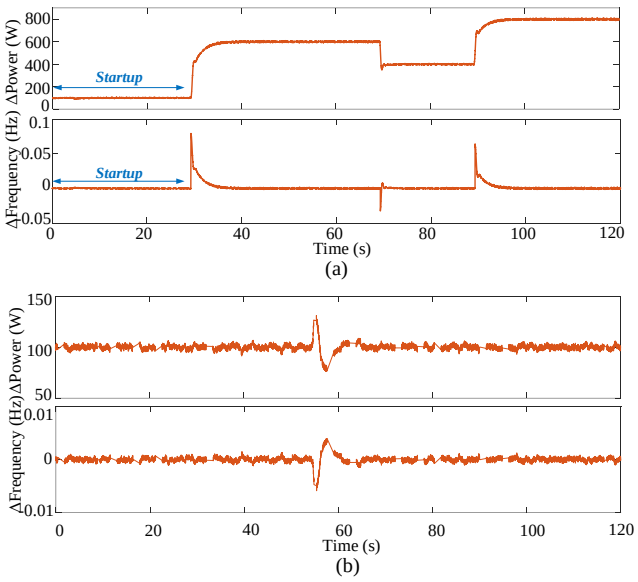

Fig. 9. Active power and frequency changes; (a) for a sequence of step changes in the reference active power; (b) for a step change in the reference voltage.

of the proposed strategy was the ability to generate dynamic outputs for control objectives. This comprises producing the control actions in the voltage control loop concerning the uncertainties and external disturbances in contrast to the traditional controllers. To track the power references and introduce damping, inertia, and droop characteristics, a VSG controller was integrated into the APC loop. Simulation results confirmed the advantages of this approach and

demonstrated its superiority over the dual-loop PI control technique.

REFERENCES

[1] R. L. de Araujo Ribeiro, A. Oshnoei, A. Anvari-Moghaddam, F. Blaabjerg, "Adaptive Grid Impedance Shaping Approach Applied for Grid-Forming Power Converters," *IEEE Access,* vol. 10, pp. 83096–83096, 2022.

[2] R. Heydari, H. Young, F. Flores-Bahamonde, S. Vaez-Zadeh, C. Gonzalez-Castano, S. Sabzevari, and J. Rodriguez, "Model-Free Predictive Control of Grid-Forming Inverters With LCL Filters," *IEEE Transactions on Power Electronics*, vol. 37, no. 8, pp. 9200–9211, Aug. 2022.

[3] M. G. Taul, X.Wang, P. Davari, and F. Blaabjerg, "An overview of assessment methods for synchronization stability of grid-connected converters under severe symmetrical grid faults," *IEEE Transactions on Power Electronics*, vol. 34, no. 10, pp. 9655–9670, Oct. 2019.

[4] T. Dragicevic, "Model predictive control of power converters for robust and fast operation of ac microgrids," *IEEE Transactions on Power Electronics,* vol. 33, no. 7, pp. 6304–6317, 2017.

[5] M. S. O. Yeganeh, A. Oshnoei, N. Mijatovic, T. Dragicevic, and F. Blaabjerg, "Intelligent Secondary Control of Islanded AC Microgrids: A Brain Emotional Learning-based Approach, " *Accepted to be published in IEEE Transaction on Industrial Electronics*, 2022. DOI: 10.1109/TIE.2022.3203677

[6] H. Young, V. A. Marin, C. Pesce, and J. Rodriguez, "Simple finite control- set model predictive control of grid-forming inverters with lcl filters," *IEEE Access,* vol. 8, pp. 81246–81256, 2020.

[7] B. Lin, L. Peng, and X. Liu, "Selective Pole Placement and Cancellation for Proportional-Resonant Control Design Used in Voltage Source Inverter," *IEEE Transactions on Power Electronics*, vol. 37, no. 10, pp. 8921–8934, Feb. 2022.

[8] R. H. Lasseter, Z. Chen, and D. Pattabiraman, "Grid-Forming Inverters: A Critical Asset for the Power Grid," *IEEE Journal of Emerging and Selected Topics in Power Electronics*, vol. 8, no. 2, pp. 925–935, Jun 2020.

[9] T. Geyer and D. E. Quevedo, "Performance OF multistep finite control set model predictive control for power electronics," *IEEE Transactions on Power Electronics*, vol. 30, no. 3, pp. 1633–1644, Mar. 2015.

[10] J. Rodriguez et al., "Latest advances of model predictive control in electrical drives Part I: Basic concepts and advanced strategies," *IEEE Trans. Power Electron.*, vol. 37, no. 4, pp. 3927–3942, 2022.

[11] M. Alhasheem, A. Abdelhakim, F. Blaabjerg, P. Mattavelli, and P. Davari, "Model Predictive Control of Grid Forming Converters with Enhanced Power Quality," *Applied Sciences*, vol. 10, no. 18, pp. 6390, 2020.

[12] A. Oshnoei, A. A. Derbas, S. Peyghami and F. Blaabjerg, "Robust Control of Voltage Source Converters: A Tube-Based Model Predictive Approach," *IEEE Transactions on Circuits and Systems II: Express Briefs*, doi: 10.1109/TCSII.2023.3259729.

[13] Y. Zhang and H. Yang, "Two-vector-based model predictive torque control without weighting factors for induction motor drives," *IEEE Transactions on Power Electronics*, vol. 31, no. 2, pp. 1381–1390, Feb. 2016.

[14] F.Wang, H. Xie, Q. Chen, S. A. Davari, J. Rodriguez, and R. Kennel, "Parallel predictive torque control for induction machines without weighting factors," *IEEE Transactions on Power Electronics*, vol. 35, no. 2, pp. 1779–1788, Feb. 2020.

[15] Y. Zhang, B. Zhang, H. Yang, M. Norambuena, and J. Rodriguez, "Generalized sequential model predictive control of IM drives with field-weakening ability," *IEEE Transactions on Power Electronics*, vol. 34, no. 9, pp. 8944–8955, Sep. 2019.

[16] M. Norambuena, J. Rodriguez, Z. Zhang, F. Wang, C. Garcia, and R. Kennel, "A very simple strategy for high-quality performance of AC machines using model predictive control," *IEEE Transactions on Power Electronics*, vol. 34, no. 1, pp. 794–800, Jan. 2019.

[17] M. Novak, H. Xie, T. Dragicevic, F. Wang, J. Rodriguez, and F. Blaabjerg, "Optimal cost function parameter design in predictive torque control (PTC) using artificial neural networks (ANN)," *IEEE Transaction on Industrial Electronics*, vol. 68, no. 8, pp. 7309–7319, Aug. 2021.

[18] L. M. A. Caseiro, A. M. S. Mendes, and S. M. A. Cruz, "Dynamically weighted optimal switching vector model predictive control of power converters," *IEEE Transaction on Industrial Electronics*, vol. 66, no. 2, pp. 1235–1245, Feb. 2019.

[19] O. Machado, P. Martin, F. J. Rodriguez, and E. J. Bueno, "A neural network-based dynamic cost function for the implementation of a predictive current controller," *IEEE Transaction on Industrial Informatics*, vol. 13, no. 6, pp. 2946–2955, Dec. 2017.

[20] H. Sorouri, A. Oshnoei, M. Novak, F. Blaabjerg, A. Anvari-Moghaddam, "Learning-Based Model Predictive Control of DC-DC Buck Converters in DC Microgrids: A Multi-Agent Deep Reinforcement Learning Approach," *Energies*, vol. 15, no. 5399, pp. 1–21, 2022.

[21] P. R. U. Guazzelli, W. C. de Andrade Pereira, C. M. R. de Oliveira, A. G. de Castro, and M. L. de Aguiar, "Weighting factors optimization of predictive torque control of induction motor by multiobjective genetic algorithm," *IEEE Transactions on Power Electronics*, vol. 34, no. 7, pp. 6628–6638, Jul. 2019

[22] Z. Zhang, W. Tian, W. Xiong, and R. Kennel, "Predictive torque control of induction machines fed by 3L-NPC converters with online weighting factor adjustment using fuzzy logic," *in Proc. ITEC*, 2017, pp. 84–89.

[23] T. Dragicevic and M. Novak, "Weighting factor design in model predictive control of power electronic converters: An artificial neural network approach," *IEEE Transaction on Industrial Electronics*, vol. 66, no. 11, pp. 8870–8880, Nov. 2019.

[24] J. He, L. Du, B. Liang, Y. Li, and C. Wang, "A coupled virtual impedance for parallel AC/DC converter based power electronics system," *IEEE Transaction on Smart Grid*, vol. 10, no. 3, pp. 3387–3400, May 2019.

[25] D. B. Rathnayake, R. Razzaghi, and B. Bahrani, "Generalized virtual synchronous generator control design for renewable power systems," *IEEE Transactions on Sustainable Energy*, vol. 13, no. 2, pp. 1021–1036, Apr. 2022.

[26] J. Fang, H. Li, Y. Tang, and F. Blaabjerg, "On the inertia of future moreelectronics power systems," *IEEE Journal of Emerging and Selected Topics in Power Electronics*, vol. 7, no. 4, pp. 2130–2146, Dec. 2019.

[27] Y. Shtessel, C. Edwards, L. Fridman, and A. Levant, *Sliding Mode Control and Observation*. New York, NY, USA: Springer, 2014.

[28] Slotine, Jean-Jacques E., and Weiping Li. Applied nonlinear control. Vol. 199. No. 1. Englewood Cliffs, NJ: Prentice hall, 1991